Science of Sintering, **54** (2022) 105-124

https://doi.org/10.2298/SOS2201105P

UDK 546.19; 546.76; 66.021.3.081.3

Removal of the As(V) and Cr(VI) from the Water Using Magnetite/3D-Printed Wollastonite Hybrid Adsorbent

Mina Popović[1*)], Zlate S. Veličković[2], Jovica Bogdanov[2], Aleksandar D. Marinković[3], Mariano Casas Luna[4], Isaak Trajković[5], Nina Obradović[6], Vladimir Pavlović[6,7]

[1]University of Belgrade, Institute of Chemistry, Technology, and Metallurgy, National Institute of Republic of Serbia, Njegoševa 12, 11000 Belgrade, Serbia
[2]Military Academy, University of Defense, Veljka Lukića Kurjaka 33, 11000 Belgrade, Serbia
[3]Faculty of Technology and Metallurgy, University of Belgrade, Karnegijeva 4, 11060 Belgrade, Serbia
[4]CEITEC Brno University of Technology, Brno, Czech Republic
[5]InnovationCenter of the Faculty of Mechanical Engineering, Kraljice Marije 16, Belgrade, 11000, Serbia
[6]Institute of Technical Sciences of SASA, 11000 Belgrade, Serbia
[7]Faculty of Agriculture, University of Belgrade, 11000 Belgrade, Serbia

Abstract:

In this study, the structure, morphology and composition of the synthesized magnetite/3D-printed wollastonite (3D_W/M) composite were characterized, and its adsorption performance with respect to As(V) and Cr(VI) were studied. Magnetite (MG) modified 3D printed wollastonite was obtained by two step procedure: modification of 3D_W with 3-aminoproylsilane (APTES) followed by controlled magnetite (MG) deposition to obtain 3D_W/M adsorbent. The structure/properties of 3D_W/M were confirmed by applying FTIR, XRD, TGD/DTA, and SEM analysis. The adsorption properties of hybrid adsorbents were carried out for As(V) and Cr(VI) removal - one relative to the initial pH value, the adsorbent mass, the temperature, and the adsorption time. Time-dependent adsorption study was best described by pseudo-second order equation, while Weber Morris analysis showed that intraparticle diffusion controled diffusional transport. Similar activation energy, 17.44 and 14.49 kJ•mol^{-1} for adsorption As(V) and Cr(VI) on 3D_W/M, respectively, indicated main contribution of physical adsorption. Determination of adsorption parameters was performed by applying different adsorption isotherm models, and the best fit was obtained using Freundlich model. The adsorption capacity of 24.16 and 29.6 mg g^{-1} for As(V) and Cr(VI) at 2^{o}C, Co = 5.5 and 5.3 mg L^{-1}, respectively, were obtained. Thermodynamic study indicated favourable process at a higher temperature. Preliminary fixed-bed column study and results fitting with Bohart-Adams, Yoon-Nelson, Thomas, and Modified dose-response model showed good agreement with results from the batch study.

Keywords*: Arsenic; Chromium; Adsorption; Magnetite; 3D-printed wollastonite.*

[*)] **Corresponding author:** mina.popovic@ihtm.bg.ac.rs

1. Introduction

The very serious problem in developing countries has become the presence of heavy metals in the water for public health. The maximal allowed concentration (MAC) for As(V) in the water decreased from 50 to 10 μg dm^{-3}, while for Cr(VI) is 50 μg dm^{-3} by considering their harmful effects on the environment and human health.

Modern human society invests significant efforts to reduce pollution and to diminish its negative influence on the environment [1,2]. Consequently, the polluted environment has a negative effect on the health and overall life quality of the human population, as well as on the existence of other living organisms. Arsenic contamination in drinking water is not such a rare case, given that over seventy countries are seriously struggling with the natural contamination of drinking water. Consumption of arsenic-contaminated water can lead to chronic arsenic poisoning causing a lot of different harmful diseases, including cancer of the lungs, bladder, liver, skin, kidneys, and cardiovascular system, as well as gastrointestinal disturbances and neurological disorders [3]. Arsenic(III) salts are very toxic and cause cancer, where the dose of 50 mg/kg is lethal. Non-toxic salts of arsenic(V) are ingredients of pesticides, as well as additives to glass that give it a green color. These salts are non-toxic and possess a strong bacterial effect. However, by ingesting large amounts, they accumulate in the body and are reduced to toxic salts of arsenic(III) [4]. The World Health Organization (WHO) has established as a drinking-water standard the concentration of arsenic in the water of 0.01 mg dm^{-3}, due to the harmful effects of arsenic on human health [5]. Chromium pollution, related to Cr(III) and Cr(VI) forms, acquire highly increasing attention due to water, soil, and air pollution. Cr(VI) is a very dangerous substance that possesses high toxicity with carcinogenic and mutagenic effects on human health [6,7]. Its ability to destroy DNA, proteins, and membrane lipids, transforming them into reactive intermediates, cause damage to the cellular functions [8]. Accordingly, based on these facts, the important global challenge has become to find out the best materials and technologies for the removal of the As(V) and Cr(VI) ions from the water. Better purification methods are preferable since changes in industrial technologies are often very limited by high investment costs. There are many different methods for the removal of heavy metal ions from water, such as coagulation, flocculation, ion exchange, membrane filtration, and separation. Modification of the surface of the inorganic materials can be physical or chemical, that enables to be adjusted for the various specific use of adsorbent for heavy metals [9]. Consequently, adsorption is the most efficient and economical method of wastewater purification [10]. There are many advantages of adsorption. Usage of different materials is one of the best benefits of adsorption, ranging from natural (organic) materials, such as cellulose, rice husk, and chitosan, to inorganic materials like ceramics with silicon oxides, composite materials, and different minerals (modified or unmodified) like wollastonite. Wollastonite is composed mainly of calcium oxide (CaO) and silicon dioxide (SiO_2), which can be responsible for the adsorption of heavy metals from the water [11]. Wollastonite as the mineral is often used as an adsorbent for the adsorption of positively charged metal ions, and also, this compound is exposed to different chemical modifications [12]. Such modifications can improve the adsorption capacity, enabling the creation of an adsorbent that can be regenerated and reused with minimal loss of its adsorption ability.

In the last few decade, the three-dimensional (3D) printing is often use, because of it is advanced additive manufacturing technique which facilitates in building up complex constructs with periodic macropores and adjustable geometrical parameters of the tested material. Also, it is useful to create the shape and the porosity of the modified materials [13,14]. Magnetite (Fe_3O_4) is known to be an effective adsorbent for several oxyanions like arsenite and arsenate [15-17], chromate [18,19] and other oxyanions (MoO_4^{2-}, $Sb(OH)_6^-$, $Sb(OH)_3$, SeO_4^{2-}, SeO_3^{2-}). Magnetite is easily synthesized on nanoscale which is useful as adsorption capacity increases with decreasing particle size of the tested material [19-22].

A recent study showed that 3D printed wollastonite showed strong selective basic catalytic properties in a dehydrogenization of the alcohols [23]. In this paper, research on adsorption characteristics of 3D_W modified with magnetite (3D-W/M) with respect to As(V) and Cr(VI) removal from water in a batch system was performed. The deposition of magnetite to 3D printed wollastonite was optimized in order to obtain the maximum adsorption capacity for As(V) and Cr(VI) ions. Optimization of the adsorption synthesis was carried out using the surface response methodology (RSM), based on two factors D-optimal design. RSM complies with the principles of environmental protection, where there is a significant decrease in the number of experiments, and consequently a decrease in waste production.

Two specific goals, achieved by two step modification of 3D printed wollastonte were: (1) creation of reactive/versatile material, amnio modified wollastonite in the first step, suitable for further modification with magnetite; (2) increasing hydrophilicity and the number of surface functionalities, obtained by precipitation of magnetite, having high affinity for oxyanions removal. The possibility of the use of 3D-W/M in a flow system was also performed in order to evaluate the possibility for application in a real system used for water purification.

2. Materials and Experimental Procedures

2.1 Materials

Detail of the material used is given in **Supplementary material**.

2.2 Synthesis 3D printed Wollastonite

Synthesis of $CaSiO_3$ powder and robocasting and sintering of porous $CaSiO_3$–SiO_2 structures 3D printed wollastonite (3D_W) was done according to Casas Luna*et. al*., using honeycomb 500 μm pore size arrangement [23].

2.3 Preparation of amino-functionalized 3D printed Wollastonite

Method applied for amino-functionalized 3D_W is given in **Supplementary material.**

2.4 Deposition of magnetite onto amino modified 3D printed Wollastonite

Detail of the deposition of MG onto 3D printed wollastonite is given in Supplementary material. Optimization procedure for **3D_W/M** synthesis was performed with respect to variable pH and $FeSO_4 \cdot 7H_2O$ concentration (Table SI).

2.5 Characterization methods

Full detail on the methods applied for characterization of the adsorbents is given in Supplementary material.

2.6 Adsorption experiments

Methodology used for determination of the adsorption performances of 3D_W/M is given in Supplementary material.

3. Results and Discussion

3.1. Adsorbent synthesis optimization

In order to design effective hybrid adsorbents for As(V) and Cr(VI) removal an optimization study was conducted. Optimization goals were directed to syntheses of adsorbent with high capacity/efficiency, improved chemical and mechanical stability of MG deposit, and fast adsorption of As(V) and Cr(VI) at operational time scale. As the most influential parameters in the synthesis of adsorbents the initial pH value of the mixture and $FeSO_4$ concentrations were selected in the optimization process to achieve the goals of optimizing the high adsorption capacity.

Amino groups are very important binding sites in the complexation process that is recently presented [24]. In the complexation/chelation interactions cations are strongly linked to amino groups, where at $pH>pH_{PZC}$ the higher value of the nucleophilicity of the amino groups brings to a stronger interaction with positive ions (cations) [25]. Hence, the amino groups covalently bonded to 3D printed wollastonite was the most important step for this modification. The total basic sites of 0.44 mmol g^{-1} found for amino modified 3D printed wollastonite play a significant role to iron binding and thus contributed to uniform magnetite loading. In order to achieve best adsorption performances an optimal procedure for MG precipitation/complexation on 3D printed wollastonite was defined by using RSM methodology.

Results of the optimized procedure of adsorbent syntheses in a batch system (*sections 2.4 and 2.6*) were applied, and also an adjustment of the volume of used solution to provide a reaction in water thin film on 3D_W surface, for syntheses of **3D_W/M**adsorbent according to the methodology described in *section 2.4*. In that way, the highest adsorption capacities were obtained at ~6% iron loaded in **3D_W/M**.

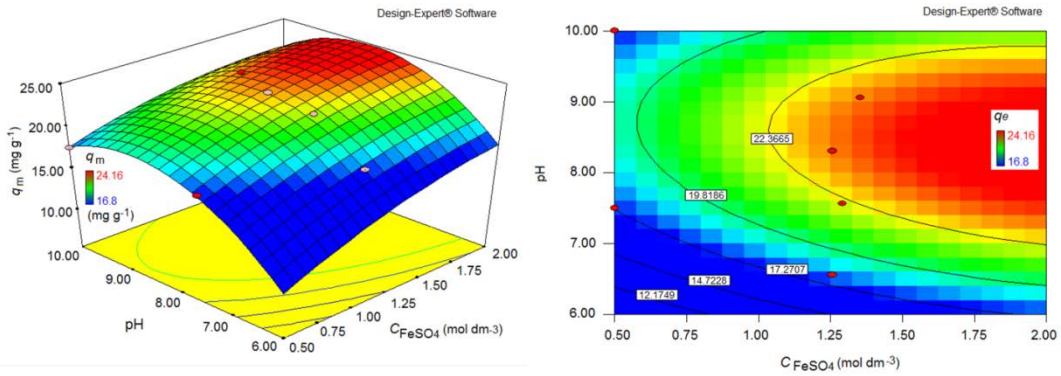

Fig. 1. The estimated surface (a) and contour (b) plots based on q_e (mg g^{-1}) for As(V) ions [$C_{i\,As(V)}$=5.5 mg dm^{-3}, m_{ads}/V=125 mg dm^{-3}, t=60 min and pH=6].

According to results from Fig. 1 and Table SI, optimal controlled precipitation and uniform distribution of MG on 3D printed wollastonite surface was achieved according to *section 2.4.2* (Supplementary material). Additionally, the porosity and pore size distribution of the sintered structures are similar to one given by Casas-Luna *et al*. [23], i.e. determined porosity of 3D_W and **3D_W/M** was 0.52 and 0.45, respectively. The obtained results indicate that magnetite deposition do not influences significant decrease of the porosity of **3D_W/M** adsorbent in relation to base material.

3.2. Adsorbent characterization

3.2.1 SEM analysis

Morphological properties and changes on the adsorbent before and after modification were monitored by scanning electron microscopy (SEM). The SEM images clearly show interconnected grains by sub-spherical pores, which size approximately was around 1.0 microns [26,27], that caused porosity of obtained material, and whose smooth surface is formed by the addition of methylhydrocyclosiloxane and sintering (Fig. 2a), before modifications, and noticeable deposits (irregularities) of magnetite after modification (Fig. 2b).

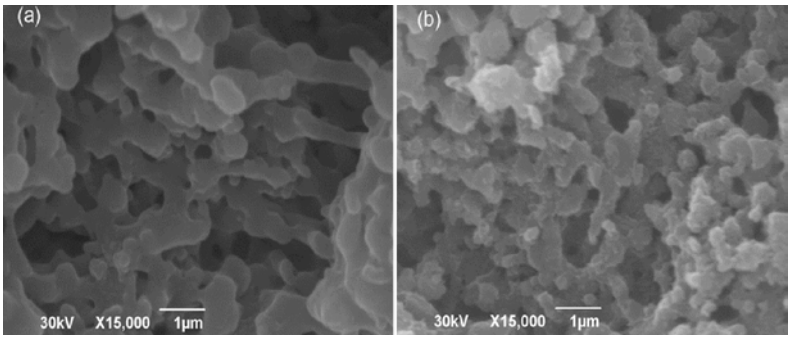

Fig. 2. SEM photographs of 3D printed wollastonite a) and b) **3D_W/M**.

3.2.2 XRD analysis

The phase composition of **3D_W/M** was studied using XRD diffractograms. On the diffractogram in Fig. 3, almost all peaks of maximum intensity at diffraction angles of 21.13°, 27.638°, 31.905°, and 45.870° appear to belong to triclinic α-wollastonite. This indicates that *β*-wollastonite is transformed into a polymorphic form during 3D printing due to the high temperature in α-$CaSiO_3$. This transformation is supported by the fact that *β*-wollastonite begins to convert to the α-form above 1125^{o}C according to the phase diagram of the CaO-SiO_2 system. It is noticeable that cristobalite at a diffraction angle of 2θ equal to 21.939°, which is a polymorphic form of silicon, begins to appear at this low temperature. Furthermore, XRD analysis [23,28,29] reveals that calcite ($CaCO_3$) at 2θ of 29.539° is present as unreacted material. It was also observed that the relatively small peak at 2θ, equal to 27,566°, belongs to pseudo-wollastonite (α-$CaSiO_3$). The diffractogram shows a series of small characteristic peaks at 2θ, (29.866°), (35.06°), (43.4°), which are well in line with the inverse cubic spinel phase of Fe_3O_4 (magnetite, JCPDS card No. 85-1436).

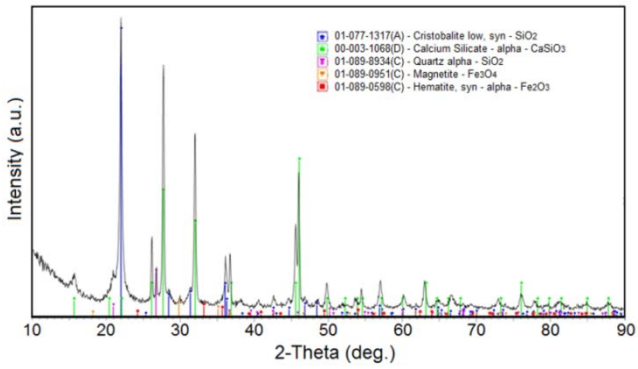

Fig. 3. XRD diffractogram of 3D printed wollastonite and **3D_W/M.**

3.2.3 TGA-DTA analysis

The DTA and TG analysis of for 3D_W is given in recently discusses by Casas-Luna *et al*. [23]. Three endothermic was noticed: first at around 115^{o}C relate to water desorption, second one at ~500^{o}C was explained as slow quartz crystallization and third one at ~840^{o}C represent phase transformation of the quartz into tridymite and/or cristobalite phase [23].

The DTA and TG curves for **3D_W/M** in the range from room to 1200^{o}C is presented on Fig. 4. Three mass changes are also visible, at different temperature intervals, of a total of 8 % in the whole interval. **3D_W/M** in DTA diagram also has a pair of characteristic peaks, the first being in the range of room temperature to 200^{o}C. There is a noticeable endothermic peak that indicates the release of moisture or the bound water from the sample (endothermic processes that mainly occur up to 200^{o}C). This process is followed by a change or with a mass drop of about 2 %. The DTA diagram shows a sharp exothermic peak at about 350^{o}C, which corresponds to the oxidation of Fe_3O_4 and the transition to Fe_2O_3. The oxidation process, the incorporation of oxygen, from the compound is followed by mass increase for~1.5 %, which is noticeable in the range of 300-400^{o}C [30].Weak endothermic peaks are visible on the DTA curve: two at about 800 and 900^{o}C, which are not followed by a change in the mass, that may correspond to the transformation of the quartz into tridymite and/or cristobalite phase [23]. The mass mass drop of about 2 % at higher temperature can be attributed to the incorporation of Fe into $CaSiO_2$, and the formation of a solid solution as well as structural rearrangement of the wollastonite into pseudo wollastonite [23].

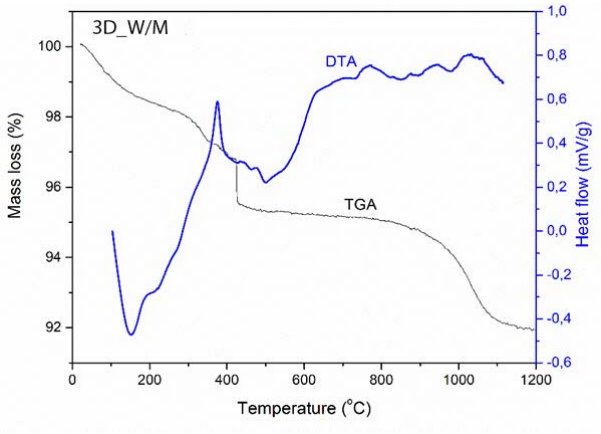

Fig. 4. Graph of changes in physical parameters in the system as a function of temperature (DTA curve blue and TGA curve black) for **3D_W/M**.

3.2.4 FTIR spectroscopy

FTIR spectra of magnetite, wollastonite, and **3D_W/M,** then **3D_W/M** loaded with Cr(VI) and As(V), are presented in Fig. 5. The bands' characteristic for wollastonite containing ceramics, observed at 982 cm^{-1}, 1054 cm^{-1}, and 1076 cm^{-1} originates from stretching vibrations of Si–O bridging groups, while bands at 935 cm^{-1}, 914 cm^{-1}, and 791 cm^{-1} originate from stretching non-bridging Si–O-Si vibrations. The intensity band at 710 cm^{-1} originates from stretching bridging Si–O-Si, which indicates the presence of a three-member ring in wollastonite-containing ceramics [27,31]. The most intensive band in the spectrum of magnetite was observed at 536 cm^{-1}. The lower intensity of this peak, observed at similar position in the FTIR spectrum of **3D_W/M**, originates from vibration of the Fe–O group [32] overlapped with Si–O-Si vibration of wollastonite structure. After As(V) and

Cr(VI) adsorption, this band is slightly shifted to 560 cm^{-1} in the spectrum of **3D_W/M**/Cr(VI) and to 550 cm^{-1} in the spectrum of **3D_W/M**/As(V).

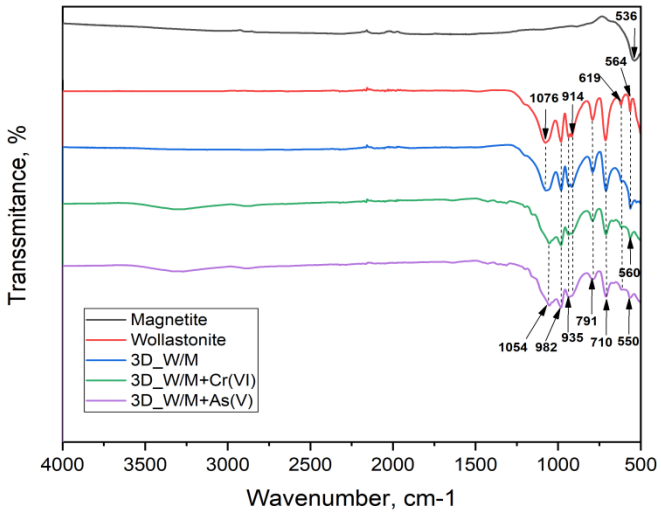

Fig. 5. FTIR spectra of magnetite, wollastonite, **3D_W/M,** mixture **3D_W/M** with Cr(VI), and mixture **3D_W/M** with As(V).

3.3. Influence of solution pH on adsorption efficiency

The effect of the solution pH on the **3D_W/M** adsorption efficiency is presented in Fig. 6. The pH change in the range from 4 to 12 was applied to study the effect of the solution of the pH on pH-dependent pollutant speciation and the generated surface charges of the adsorbent, i.e.the efficiency of the adsorption.In aqueous systems, the surface of MG is covered with FeOH groups that can be protonated or deprotonated and generate surface charge $FeOH_2^+$ or FeO^- at pH values below or above the point of zero charge for magnetite (pH_{PZC}), respectively [33]. Electrostatic forces between metal ion species and surface charges are responsible for adsorption [33,34]. The point of zero charge for magnetite is the pH value at which the surface concentrations of $FeOH_2^+$ and FeO^- groups are equal. According to that the adsorption capability of **3D_W/M** depends on both the, it is necessary to determine the $pH_{PZC.}$The measured pH_{PZC} of unmodified WL was 2.7, while pH_{PZC} of MG modified 3D_W based adsorbents was 7.2 (**Fig. S1**) [31].

The dependence of adsorption efficiency of the oxyanions As(V) and Cr(VI) removal versus the initial pH on **3D_W/M** is given in Fig. 6.

On the other side, oxyanions that are negatively charged could be effectively bonded to positively charged **3D_W/M** surface at the $pH<pH_{PZC}$ (Fig. 6). Hence, the applicability of the **3D_W/M** depends on the initial pH solution where the adjustment of the pH of the inlet water determinates the adsorption efficiency.It could be noted low dependence of As(V) and Cr(VI) on **3D_W/M** in the pH adsorption efficiency range from 4-6with > 85 % removal, and subsequently, the gradual decrease is observed at pH>7. The pH-dependent successive ionization of triprotic arsenic acid (H_3AsO_4) can be presented by the following equilibrium [35]:

$$H_3AsO_4 \xrightleftharpoons{pK_{a(1)} = 2.24} H^+ + H_2AsO_4^- \xrightleftharpoons{pK_{a(2)} = 6.69} 2H^+ + HAsO_4^{2-} \xrightleftharpoons{pK_{a(3)} = 11.5} 3H^+ + AsO_4^{3-}$$

Similar equilibria could be given for chromic acid:

$$H_2CrO_4 \xrightleftharpoons{pK_{a(1)} = -0.98} H^+ + HCrO_4^- \xrightleftharpoons{pK_{a(2)} = 6.49} 2H^+ + CrO_4^{2-}$$

And also participating equilibrium in acidic condition (pH 0-7, Ka = 3.4-5.0 × 10^{14}) [36]:

$$2H^+ + 2CrO_4^{2-} \rightleftharpoons Cr_2O_7^{2-} + H_2O$$

The crucial role in the adsorption processes is the presence of the molecular forms at pH<2 and the equilibrium of the arsenic ions in the different forms at the higher pH [37]. Weak arsenous acid as well as chromic acid effectively interacts with **3D_W/M** at pH in the vicinity of p*K*a [38]. At the pH<pH_{PZC} the negatively charged As(V) species, *i.e.* $H_2AsO_4^-$ and $HAsO_4^{2-}$ (Fig. 6), and Cr(VI) species, *i.e.* $HCrO_4^-$ and CrO_4^{2-} (Fig. 6), could participate in an electrostatic attraction with the positively charged adsorbent surface. Oppositely, the low adsorption efficiency is caused by electrostatic repulsion at pH>pH_{PZC}.

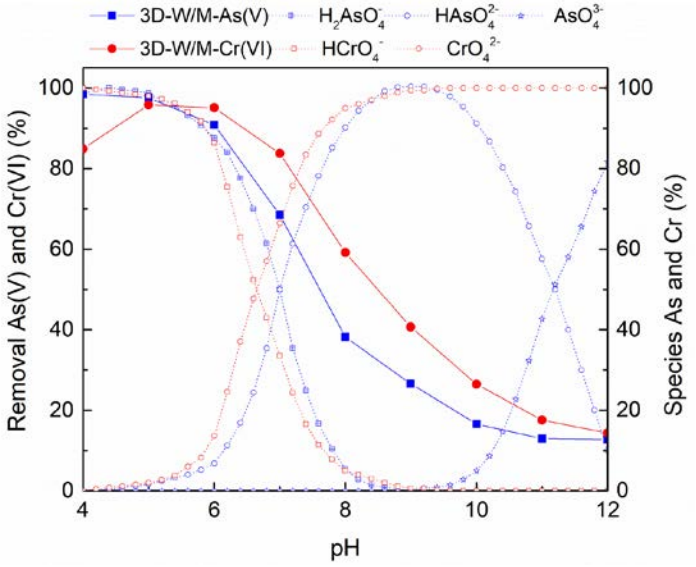

Fig. 6. The influence of pH on the adsorption of Cr(VI) and As(V) ions on **3D_W/M** (in %) [$C_{i[Cr(VI)]}$= 5.3 mg dm^{-3},$C_{i[As(V)]}$= 5.5 mg dm^{-3}, m/V = 1250 mg dm^{-3} and T = 25°C].

Consequently, three factors determine choice of the initial pH 6: the adsorption capacity, adsorbent stability, and pH of natural water used as inlet water in the adsorption experiment (avoidance of inlet water pH adjustment). The higher hydrolytic stability of the surface functionalities, long-term adsorbent usability, in the pH range nearby neutral and weak base environment, from pH 6 to 8, are very important characteristics of the adsorbent that are of great importance the economic and technological aspects. The determined pH_{PZC} and pH dependent adsorption study corroborate selection of optimal operative pH to be ~6.2.

3.4. Adsorption kinetics

The study of kinetics provides an insight into the possible mechanism of adsorption along with the reaction pathways. The effect of the time on the adsorption of arsenate ions was monitored in the range of 5 to 120 minutes for As(V), while for the Cr(VI) ions, the equilibrium was established after 70 minutes. In order to interpret the adsorption mechanism, pseudo-first, pseudo-second-order, and second-order models as well as the Weber Morris

diffusion model [39] was used for modelling kinetic data. Details on the models used are given in the **Supplementary material, Table SII and SIII (eq. S5-eq. S11**). According to the regression coefficient (R^2) and the calculation of the standard error for all the model parameters, the experimental kinetic data is the best described using a pseudo-second-order model (**Equation S6**). The kinetic parameters for adsorption of As(V) and Cr(VI) on **3D_W/M** adsorbent are shown in Table I.

Tab. I Pseudo-first, PSO and second order model parameters for the adsorption of As(V) and Cr(VI) on to **3D_W/M** ($C_{i\,[As(V)]}$ = 5.5 mg dm^{-3}, $C_{i\,[Cr(VI)]}$ = 5.3 mg dm^{-3}; pH = 6.0; m/V = 125 mg L^{-1}, T = 298 K).

Adsorbent	Ion	Parameter	Pseudo-first	PSO	Second order
3D_W/M	As(V)	q_e	15.357	28.177	28.177
		k (k_1, k_2)	0.0328	0.0042	0.0036
		R^2	0.818	0.996	0.797
	Cr(VI)	q_e	23.804	29.117	29.117
		k (k_1, k_2)	0.0149	0.00621	0.0049
		R^2	0.853	0.995	0.859

Additionally, the rate of adsorption steps was determined using the Weber-Morris (W-M), Dunwald-Wagner, and Homogenous Solid Diffusion Model (HSDM) (**Table SIII**). The obtained model parameters are given in Table II.

Tab. II Kinetic parameters of the W-M, D-W and HSDM models for the adsorption of As(V) and Cr(VI) onto **3D_W/M.**

Model	Parameter	As(V)	Cr(VI)
Weber-Morris (W-M) (Step 1)	k_{p1} (mg g^{-1} $min^{-0.5}$)	4.144	2.4302
	C (mg g^{-1})	1.329	10.528
	R^2	0.996	0.995
Weber-Morris (Step 2)	k_{p2} (mg g^{-1} $min^{-0.5}$)	0.0703	0.415
	C (mg g^{-1})	23.612	22.981
	R^2	0.997	0.996
Dunwald-Wagner (D-W)	K	0.0232	0.0333
	R^2	0.821	0.870
Homogenous Solid Diffusion Model	Ds	2.86×10^{-11}	3.9×10^{-11}
	R^2	0.812	0.869
Bangham's kinetic model	k	0.483	0.373
	á	2.574	2.614
	R^2	0.939	0.934

The complex nature of the adsorption process was considered either as a single step, as described by the pseudo-second-order equation, or can be described by consecutive/competitive steps. The Weber-Morris method reveals two linear steps that describe the adsorption process: fast kinetics in the first step and slower in the second. The first linear part describes the external mass transfer to the adsorbent surface, while the second part describes the process of material transfer to the porous structure of the adsorbent, and strictly depends on the dimensions and shape of the pores and the density of their network on the adsorbent **3D_W/M**. Intra-particle and film diffusion slow down the transport of adsorbates. In the final phase of the process, adsorption is slow until the saturation on the entire available surface of the adsorbent is achieved. The value of constant *C* from W-M

model indicates that intra-particle diffusion is the main limiting process to overall pollutant transport in the adsorption process.

Kinetic data can be additionally used to check whether the pore diffusion is an only rate-controlling step or not. If the experimental data are represented by this equation, the adsorption kinetics is described by using pore diffusion Bangham's equation (**S11**). From the results of non-linear fitting between the experimental values and the predicted values for the **3D_W/M**/As(V) and **3D_W/M**/Cr(VI) system (R^2 = 0.939 and 0.934) may be concluded that the diffusion of adsorbate into pores of the studied adsorbents is not the only rate controlling step, as stated by others [40].

3.5. Adsorption activation energy

In relation to the results of kinetic research performed at temperatures of 298, 308, and 318 K (**Table SIV**), it is possible to determine the activation energy using the Arrhenius equation (**S12**). The value of activation energy occurs as a reason for the mechanism of metal-ion adsorption on the adsorbent used. Physisorption or physical adsorption generally possesses energy up to 40 kJ·mol^{-1}, while chemisorption requires a higher energy and activation energy over 40 kJ mol^{-1}. Based on the obtained results where E_a = 17.44 and 14.49 kJ·mol^{-1} for adsorption As(V) and Cr(VI) on **3D_W/M**, respectively, it can be concluded that the main mechanism of adsorption is physical adsorption.

3.6. Adsorption isotherm

The state of interactions/bonds on the surface of the adsorbate/adsorbent can bev analyzed by fitting the experimental data with different adsorption isotherms. The normalized correlation coefficient and standard deviation were used to estimate the fit of the adsorption data. The data obtained from the experiments were compared with the models of Langmuir, Freundlich, Temkin, Dubinin-Radushkevich, and Toth isotherms (**Table SV**), the parameters of which are shown in Table III. In order to fit the experimental adsorption data with the isotherm models, nonlinear regression was used; the normalized standard deviation Δq was calculated together with the correlation coefficient R^2. By analyzing the experimental data on the adsorption of As(V) and Cr(VI) ions on the tested adsorbent, the best fit is given by the Freundlich isothermal model Figs. 7 and 8. According to the Freundlich isotherm, the mechanism of ion adsorption at 3D_W/M can be described as heterogeneous adsorption, where the adsorbed ions have different enthalpies and adsorption activation energies. The value of n from the Freundlich isotherm is a measure of adsorption intensity or surface heterogeneity. Values of n close to zero indicate a highly heterogeneous surface. Values of n <1 imply a chemisorptions process, and higher values (Table III) indicate combined adsorption, e.g. physisorption and chemisorption with different process contributions at different system balancing steps. The apparent energy of absorbent adsorption onto **3D_W/M** is found out by using Dubinin–Radushkevich isotherm. Gaussian energy distribution onto a heterogeneous surface [41] is usually used to express the adsorption mechanism by applying the model. It has often successfully fitted into the intermediate-range of concentrations data properly and high solute activities. As the mean free energy expresses the energy for taking out a molecule from its location in the sorption space to the infinity, the model was usually useful to distinguish the physical and chemical adsorption of ions with its mean free energy, i.e. *E*, per molecule of adsorbate. The value *E* from the DR isotherm can be used to predict the reaction mechanism where adsorption energies < 8 KJ mol^{-1} indicate physisorption, in the range 8 to 16 KJ mol^{-1} dominate ion exchange, and > 16 KJ mol^{-1} prevail chemisorptions [42]. The obtained *E*a values from 7,735 to 7,805 indicate that physisorption is the most contributing mechanism in the sorption of As(V) on **3D_W/M**. While obtained *E* a values

from 8.0 to 8.05 indicate that the combined mechanism of physisorption and ion exchange is the determining mechanism in the sorption of Cr(VI) on **3D_W/M**.

Tab. III Parameters of adsorption isotherms for As(V) and Cr(VI) adsorption on **3D_W/M.**

Isotherm model and parameters		As(V)			Cr(VI)		
		25°C	35°C	45°C	25°C	35°C	45°C
Langmuir isotherm	q_m (mg g^{-1})	24.08	25.744	27.058	31.46	32.08	34.78
	K_L (dm^3 mg^{-1})	5.206	5.553	6.319	5.650	5.759	6.021
	K_L (dm^3 mol^{-1})	270691	288734	328563	423298	431464	451093
	R^2	0.908	0.904	0.918	0.929	0.930	0.941
Freundlich isotherm	K_F (mg g^{-1}) (dm^3 mg^{-1})$^{1/n}$	18.349	20.015	22.337	25.117	25.859	29.038
	1/n	3.129	3.116	3.277	2.695	2.679	2.559
	R^2	0.994	0.993	0.984	0.997	0.997	0.997
Temkin isotherm	A_T (dm^3 g^{-1})	126.56	149.97	206.31	132.04	136.27	135.19
	b (mg g^{-1})	3.89	4.04	4.20	4.96	5.03	5.49
	B_T (J mol^{-1})	637.39	634.44	630.01	500.1	508.9	481.4
	R^2	0.964	0.957	0.965	0.941	0.939	9.366
Dubinin-Radushkevich	q_m (mg g^{-1})	17.59	18.49	20.44	21.20	21.57	23.32
	K_{ad} (mol^2	8.36	8.31	8.21	7.80	7.79	7.71
	E (KJmol^{-1})	7.735	7.758	7.805	8.00	8.01	8.05
	R^2	0.906	0.904	0.923	0.915	0.916	0.923
Toth	q (mg g^{-1})	13.712	14.691	17.298	16.979	17.390	19.105
	K_L(mg g^{-1})	45.792	50.734	45.406	56.941	58.530	51.805
	n(mg g^{-1})	0.720	0.714	0.748	0.662	0.695	0.646
	R^2	0.998	0.996	0.990	0.999	0.999	0.999

Non-linear isotherms model fitting for As(V) and Cr(VI) removal using **3D_W/M** are given on(Fig. 7)and (Fig. 8), respectively.

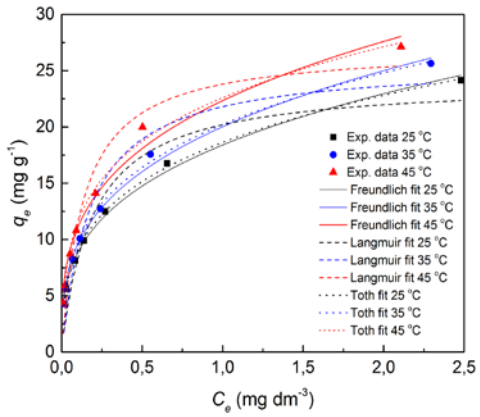

Fig. 7. Non-linear fit using Freundlich, Langmuir and Toth isotherm for As(V) adsorption on **3D_W/M.**

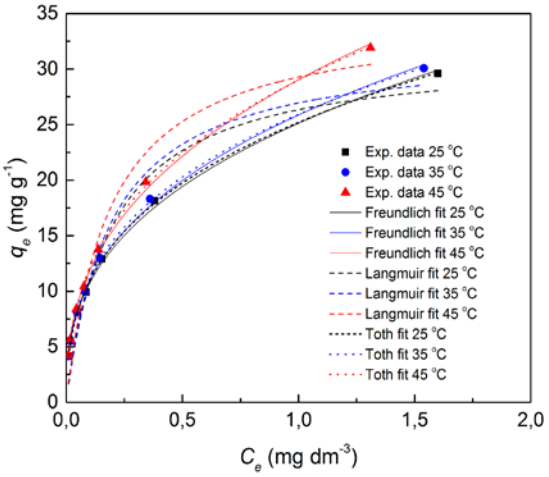

Fig. 8. Non-linear fit using Freundlich, Langmuir and Toth isotherm for Cr(VI) adsorption on **3D_W/M.**

Even the results from non-linear model fitting, using Langmuir equation, are of lower statistical validity, in comparison to Freundlich, they are in good agreement with result obtained from Figs. 7 and 8, *i.e.* isotherm model calculation for specific condition: As(V), *C*o=5.5 mg L^{-1}; m/V = 125 mg L^{-1}, 25°C *q*= 24.16, 35°C *q*=25.65 and 45°C *q* = 27.136 mg g^{-1} , and Cr(VI) *C*o=5.3 mg L^{-1}; m/V = 125 mg L^{-1}, 25°C *q* = 29.60, 35°C *q*= 30.08 mg g^{-1} and 45°C *q* = 31.92 mg g^{-1} .

3.7. Thermodynamic studies

Gibbs free energy (ΔG^{Θ}), enthalpy (ΔH^{Θ}), and entropy (ΔS^{Θ}) are calculated by Van't Hoff equation (1) and (2):

$$\Delta G^{\Theta} = -RT\ln(b) \qquad (1)$$

$$\ln(b) = \frac{\Delta S^{\Theta}}{R} - \frac{\Delta H^{\Theta}}{(RT)} \qquad (2)$$

where *T* is the absolute temperature in K, R is the universal gas constant (8.314 mol^{-1} K^{-1}) and the adsorption constant *b* is calculated using the Langmuir isotherm (Table IV). The ΔH^{Θ} and ΔS^{Θ} were calculated from the slope and sections in the diagram ln(*b*) - T^{-1}, assuming that the adsorption kinetics are stationary. The calculated thermodynamic parameters are shown in Table IV.

Tab. IV Calculated Gibbs free adsorption energy, enthalpy, and entropy for adsorption As(V) and Cr(VI) on **3D_W/M** at 298, 308, and 318 K.

Ion	**ΔG^{Θ} (kJ mol^{-1})**			**ΔH^{Θ} (kJ mol^{-1})**	**ΔS^{Θ}(J mol^{-1} K^{-1})**	**R^2**
	298 K	308K	318K			
As(V)	-40.96	-42.50	-44.22	7.61	162.82	0.957
Cr(VI)	-42.07	-43.53	-45.06	2.50	149.44	0.942

The negative adsorption standard of free energy (ΔG^{Θ}) and positive standard values of entropy (ΔS^{Θ}) at all temperatures indicate that the adsorption process takes place

spontaneously [38,43]. A decrease in the Gibbs free energy (ΔG^{Θ}) with an increase in temperature also indicates the spontaneity of the reaction increases with temperature increase. Positive values of ΔS^{Θ} indicate a tendency of greater disorder of the **3D_W/M** surface system and As(V) and Cr(VI) solution. A positive value of enthalpy (ΔH^{Θ}) indicates that adsorption is an endothermic process. According to generally accepted interpretations, changes in the enthalpy value may indicate the nature of the adsorption mechanism. A change in enthalpy between 2 and 21 kJ mol^{-1} indicates physical adsorption (Table IV), while a change in enthalpy in chemisorption is in the range between 80–200 kJ mol^{-1}.

3.8. Adsorption mechanism

The possible adsorption mechanism is complex and could be presented as it is given in Fig. 9. It was explained that dominant surface complexes were formed between one adsorbed arsenate oxyanion and two FeO_6 octahedra on surfaces of magnetite [44-46]. In a similar fashion, the $H_2AsO_4^-$ and $HAsO_4^{2-}$ could be linked *via* the oxygen atoms to magnetite iron by forming either monodentate mononuclear or bidentate binuclear complexes. Ligand exchange is a process at surface which produces formation of monodentate complex, while the next slowstepprepresents a second ligand exchange resulting in the formation of an inner-sphere bidentate binuclear complex [47].

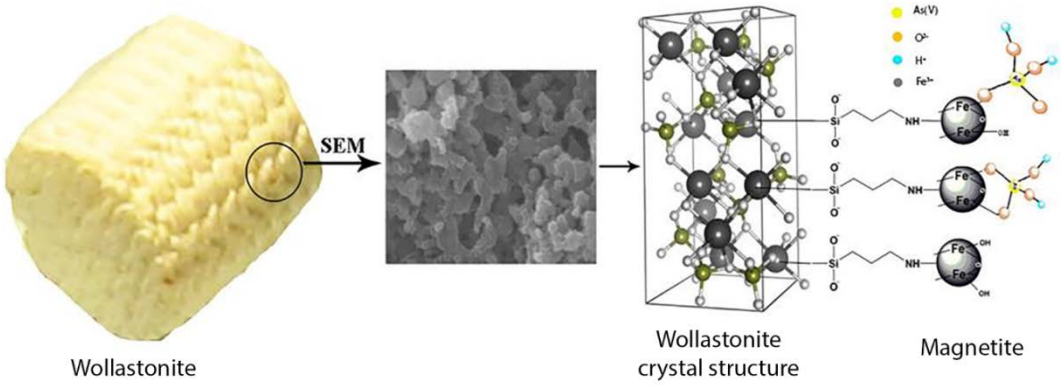

Fig. 9. Adsorption mechanism of As(V) ions on **3D_W/M.**

Except for this, experiments performed with **3D_W/M** in the presence of a different concentrations of KCl (0.5, 1 and 3 mg L^{-1}), led to somewhat enhanced As(V) and Cr(VI) removal (in the range 2-5 %). The increase of the negative charge in the electrical double layer is due to the biding of negatively charged As(V) and Cr(VI) species [47], where the higher ionic strength of the solution, increased concentration of counterions could compensate the surface negative charges. This result corroborate that the main adsorption mechanism is the formation of the inner-sphere complexes [48]. Additionally, the low influence of interfering ionsand pH_{PZC} decreases after adsorption (pH_{PZC} after adsorption of arsenate 6.6 and chromate 6.4) are the properties indicative of the formation of inner-sphere surface complexes [49]. Thus, formation of inner-sphere complexes is the process of the high probability, while the interactions between the As(V) and Cr(VI)species and the protonated hydroxyl groups lead to the formation of the outer sphere due to electrostatic interactions [50]. In general complex mechanism operates where surface complexation with contribution of physical adsorption, i.e. electrostatic interactions, is of utmost contribution to overall mechanism.

3.9. Adsorption performances of 3D_W/M in a flow system

The behaviour of the adsorbate solution under dynamic conditions is difficult to describe. Due to the difficulty of finding the right model, four different flow adsorption models were used (detail description is given in **Supplementary material, eqs. (S18) – (S24)**. The maximum adsorption capacity q_{exp} (mg g^{-1}) of the adsorption A (V) and Cr(VI) on **3D_W/M**, for the given parameters, can be calculated from the experimental data, i.e. the area under the breakthrough curve. This was done by multi-parameter nonlinear modelling of the breakthrough curve using one of the selected models, and fitting using commercial software Origin 8. The most commonly used models are Bohart-Adams, Yoon-Nelson, Thomas, and Clark, results are shown in **Fig. S2** and given in Table V.

Tab. V Column adsorption parameters for As(V) and Cr(VI) onto **3D_W/M**($C_{0[As(V)]}$ = 5.50 mg dm^{-3}; $C_{0[Cr(VI)]}$ = 5.30 mg dm^{-3} ; m_{ads} = 1.08 g; t=25°C; pH=6, flow rate 1.0 cm^3min^{-1}).

Model	Ion		As(V)	Cr(VI)
Bohart-Adams model	k_{BA}	dm^3 mg^{-1} min^{-1}	0.181	0.156
	q_o	mg g^{-1}	21.358	24.823
	R^2		0.998	0.997
Yoon-Nelson model	k_{YN}	min^{-1}	0.995	0.829
	θ	min	4.194	5.056
	R^2		0.998	0.996
Thomas model	k_{Th}		0.181	0.156
	q_o	mg g^{-1}	21.358	24.812
	R^2		0.998	0.999
Clarke model	A		22.287	7.052
	r	min^{-1}	0.884	0.656
	n		1.649	1.348
	R^2		0.998	0.999

According to the results given in Table V, it could be deduced that the column with **3D_W/M** shows acceptable performances. Initially, in the continuous flow maximum removal occurs at the top of the column until the adsorbent becomes saturated (**Fig. S2**). After that, the adsorption zone gradually moves downward and eventually reaches the exit of the bed, when concentrations of the adsorbate in the effluent and the influent become equal. Fast saturation of the bed occurred after the breakthrough point, which is evident from the steep gradient of the curve in **Fig. S2**. Total adsorbed As(V) or Cr(VI) (q_m) in the column were a little bit lower than in the batch system, which is similar to other research results [37,51,52].

3.10. Comparative analysis of the adsorption performance of 3D_W/M with literature data

In order to recognize the benefits of the possible use of the **3D_W/M** in the water purification processes, the data from the literature were compared with results obtained from this study (Table VI).

According to the results presented in Table VI the absorption capacity of **3D_W/M** (23.873 mg g^{-1}) for removal of the As(V) from the water, compared with q_{max} values of materials e-MWCNT/Fe^{2+} [38] possess a similar adsorption capability, while compared with DFH [55], 3D_W/M showed a better adsorption capability.

Also, the adsorption capacity of **3D_W/M** at pH 6.4, was higher than that of the materials zinc oxide nanocrystal-decorated regenerated micro-fibrillated cellulose scaffolds (from jute) [56], for removal of As(V) with adsorption capacity of 4.421 mg g^{-1}. Interestingly, three materials, adsorbents NC-MA/ L-MG[54], Magnetite [54] and PEI-Al_2O_3 [53], on the pH_{pzc} similar to **3D_W/M**, showed the higher adsorption capacity 85.3 mg g^{-1}, 91.2 mg $g^{-1}$and 61.3 mg g^{-1}, respectively, than in the material **3D_W/M,** whileMC-O/NC-L-MG [54] showed the lower value of the adsorption capacity, 18.5 mg g^{-1}.

Tab. VI Material properties and adsorption capacities of different adsorbents.

Ion	Adsorbent	pH_{pzc}	Capacity	Reference
As(V)	PEI-Al_2O_3	6.2	61.3 mg g^{-1} (pH 6)	[53]
As(V)	**3D_W/M**	7.2	23.873 mg g^{-1} (pH 6.2)	This paper
As(V)	NC-MA/ L-MG	$6.5^a/5.7^b$	85.3 mg g^{-1}(pH 6.0)	[54]
As(V)	MC-O/NC-L-MG	$6.1^a/5.8^b$	18.5 mg g^{-1}(pH 6.0)	[54]
As(V)	Magnetite	$6.6^a/5.9^b$	91.2 mg g^{-1}(pH 6.0)	[54]
As(V)	e-MWCNT/Fe^{2+}	7.5	23.47 mg g^{-1}(pH 4.0)	[38]
As(V)	Dust Ferric Hydroxide (DFH)	5.3	6.9 mg g^{-1} (pH 7.9)	[55]
As(V)	Zinc-oxide nanocrystal-decorated regenerated micro-fibrillated cellulose scaffolds (from jute)	/	4.421 mg g^{-1}(pH 7.0)	[56]
As(V)	Magnetite/Starch	6.1	248 mg g^{-1} (pH 5.0)	[57]
As (V)	NC-PEG/FO	$8.5^a/7.6^b$	26 mg g^{-1}(pH 6.9)	[22]
Cr(VI)	Propyrrole/monodispersed Latex sphere (PPy/MLS)	4.6	343.64 mg g^{-1} (pH 2.0)	[58]
Cr(VI)	PPy/OMWCNTs NCs	/	294 mg g^{-1} (pH 2.0)	[59]

a - before adsorption, b- after adsorption

On the other hand, the adsorption capacity for the removal of the As(V) at the weak acidic conditions pH (4-6) of Magnetite/Starch was 248 mg g^{-1}[57]. Also, for removal of the As(V) from the water using NC-PEG/FO [22], the adsorption capacity 26 mg g^{-1}. Finally, polypyrrole/monodispersed latex sphere (PPy/MLS) for removal of the Cr(VI) from the water [58] had the adsorption capacity 343.64 mg g^{-1} at pH 2.0, while the PPy/OMWCNTs NCs had the adsorption capacity 294 mg g^{-1}, on the same pH value [59]. Scientific results that we obtained from this study, should be applied in the real system for the water purification, the removal of the As(V) ions form the water, as well as, comparative analysis that justifies the application of the **3D_W/M** in this area.

4. Conclusion

In this work 3D printed wollastonite, obtained using the 3D printing technique and modified with magnetite showed high adsorption performances for oxyanions removal from water. FTIR, XRD, TGA/DTA, and SEM techniques confirmed the wollastonite phase and the successfulness of magnetite precipitation. Likewise, the SEM analysis confirmed porosity of **3D_W** support and formation of MG aggregates in the course of deposition process. The adsorption properties of the hybrid adsorbent largely depended on the surface properties of magnetite which was achieved by the controlled process of magnetite deposition on 3D

printed wollastonite. Based on the obtained results, it can be found that the process of arsenic and chromium oxyions adsorption can be best described by the Freundlich model of the adsorption isotherm, which indicates multilayer adsorption. Also, low value of the adsorption enthalpy indicates endothermic character of the process and higher adsorption capacity at higher temperature. Experimental data obtained from kinetic experiments were fitted using pseudo-first, pseudo-second, and second order, where the best description of the kinetic was obtained using second-order rate constant. According to results presented, it was found the As(V) and Cr(VI) adsorption mechanism was complex process with contribution of both physical and chemical adsorption, i.e. formation of inner sphere complexes. Also, comparing the obtained results with the results of other authors, it can be noticed that **3D_W/M** adsorbent showed satisfactory adsorption performances and potential applicability in column system.

Acknowledgments

This work was financially supported by the Ministry of Education, Science and Technological Development of the Republic of Serbia (Contract Numbers. 451-03-9/2021-14/200026, 451-03-9/2021-14/200135, and 213-1/21 -08-03-2021).

5. References

1. S. S. Stupar, M. M. Vuksanović, L. M. Totovski, R. M. Jančić Heinemann, D. Ž. Mijin, Adsorption of anthraquinone dye ab111 from aqueous solution using synthesized alumina-iron oxide doped particles, Sci Sinter, 53 (2021) 91–117.
2. D Jeremić, L Andjelković, M. R. Milenković, M. Šuljagić, M. Š. Ristović, S. Ostojić, A. S. Nikolić, P. Vulić, I. Brčeski, V. Pavlović, One-pot combustion synthesis of nickel oxide and hematite: From simple coordination compounds to high purity metal oxide nanoparticles, Sci Sinter, 52 (2020) 481–490.
3. K. Jomova, Z. Jenisova, M. Feszterova, S. Baros, J. Liska, D. Hudecova, C. J. Rhodes, M. Valko, Arsenic: Toxicity, oxidative stress and human disease, J Appl Toxicol 31 (2011) 95–107.
4. P. V. Nidheesh, T S. A Singh, Arsenic removal by electrocoagulation process: Recent trends and removal mechanism, Chemosphere, 181 (2017); 418–432.
5. S. Yamamura, Drinking water guidelines and standards. United Nations Synth Rep Arsen Drink Water 2001:18.
6. W. Jiang, Q. Cai, W. Xu, M. Yang, Y. Cai, D. D. Dionysiou, K. E. O'Shea, Cr(VI) adsorption and reduction by humic acid coated on magnetite, Environ Sci Technol, 48 (2014) 8078–8085.
7. G. Chen, C. Qiao, Y. Wang, J. Yao, Synthesis of magnetic gelatin and its adsorption property for Cr(VI). Ind Eng Chem Res, 53 (2014) 15576–15581.
8. G. De Mattia, M. C. Bravi, O. Laurenti, O. De Luca, A. Palmeri, A. Sabatucci, G. Mendico, A. Ghiselli, Impairment of cell and plasma redox state in subjects professionally exposed to chromium, Am J Ind Med, 46 (2004) 120–125.
9. J. Perendija, Z. S. Veličković, Lj. Dražević, I. Stojiljković, M. Milčić, M. M. Milosavljević, A. D. Marinković, V. Pavlović, Evaluation of adsorption performance and quantum chemical modeling of pesticides removal using Cell-MG hybrid adsorbent, Sci. Sinter., (2021) in press.
10. N. Amin, S. Kaneco, T. Kitagawa, A. Begum, H. Katsumata, T. Suzuki, K. Ohta, Removal of arsenic in aqueous solutions by adsorption onto waste rice husk, Ind Eng Chem Res, 45 (2006) 8105–8110.

11. Y. C. Sharma, Adsorption of Cr (VI) onto wollastonite: Effect of pH. Indian J Chem Technol, 8 (2001) 186–190.
12. A Hedström, Wollastonite as reactive filter medium for sorption of wastewater ammonium and phosphorus, Environ Technol, 27 (2006) 801–809.
13. H. Shao, X. Yang, Y. He, J. Fu, L. Liu, L. Ma, L. Zhang, G. Yang, C. Gao, Z. Gou, Bioactive glass-reinforced bioceramic ink writing scaffolds: sintering, microstructure and mechanical behavior, Biofabrication, 7 (2015) 035010.
14. B. G. Compton, J.A. Levis, 3D-printing of light weight cellular composite, Adv. Mater, 26 (2014) 5930-5935.
15. Shipley, H. J.; Yean, S.; Kan, A. T.; Tomson, M. B., Adsorption of Arsenic to Magnetite Nanoparticles: Effect of Particle Concentration, pH, Ionic Strength, and Temperature. Environ. Toxicol. Chem., 28, (2009) 509-515.
16. Mamindy-Pajany, Y.; Hurel, C.; Marmier, N.; Rom´eo, M., Arsenic (V) Adsorption from Aqueous Solution onto Goethite, Hematite, Magnetite and Zero-Valent Iron: Effects of pH, Concentration and Reversibility. Desalination, 281(2011) 93-99.
17. Lunge, S.; Singh, S.; Sinha, A. Magnetic Iron Oxide (Fe_3O_4) Nanoparticles from TeaWaste for Arsenic Removal. J. Magn. Magn. Mater., 356(2014) 21-31.
18. Gallios, G. P.; Vaclavikova, M. (2008) Removal of Chromium (VI) from Water Streams: A Thermodynamic Study. Environ. Chem. Lett., 6 (2008) 235-240.
19. Yuan, P.; Liu, D.; Fan, M. D.; Yang, D.; Zhu, R. L.; Ge, F.; Zhu, J. X.; He, H. P. Removal of Hexavalent Chromium Cr(VI) from Aqueous Solutions by the Diatomite-Supported/Unsupported Magnetite Nanoparticles. J. Hazard. Mater., 173 (2010) 614-621.
20. Petrova T. M.; Fachikov L.; Hristov J. The Magnetite as Adsorbent for some Hazardous Species from Aqueous Solutions: A Review. Int. Rev. Chem. Eng., 3 (2011) 134-152.
21. Taleb K, Markovski J, Milosavljević M, Marinović-Cincović M, Rusmirović J, Ristić M, Marinković A, Efficient arsenic removal by cross-linked macroporous polymer impregnated with hydrous iron oxide: material performance. Chem Eng J, 279 (2015) 279–278.
22. Khaled a. Taleb, J Rusmirović, M. Rančić, J. Nikolić, S. Drmanić, Z. Veličković and A. Marinković, Efficient pollutants removal by amino-modified nanocellulose impregnated with iron oxide, J. Serb. Chem. Soc., 81 (2016) 1199–1213.
23. M. Casas-Luna, J.A. Torres-Rodríguez, O. U. Valdés-Martínez, N. Obradović, K. Slámečka, K. Maca, J. Kaiser, E. B. Montúfar, L. Čelko, Robocasting of controlled porous $CaSiO_3$–SiO_2 structures: Architecture – Strength relationship and material catalytic behavior, Ceram Int, 46 (2020) 8853–8861.
24. S. E. Cabaniss, Forward modeling of metal complexation by NOM: II. Prediction of binding site properties, Environ Sci Technol, 45 (2011) 3202–3209.
25. G. D. Vuković, A. D. Marinković, S. D. Škapin, M. T. Ristić, R. Aleksić, A. A. Perić-Grujić, P. S. Uskoković, Removal of lead from water by amino modified multi-walled carbon nanotubes, Chem Eng J, 173 (2011) 855–865.
26. R. PS. Chakradhar, B. M. Nagabhushana, G. T. Chandrappa, K. P. Ramesh, J. L. Rao, Solution combustion derived nanocrystalline macroporous wollastonite ceramics, Mater Chem Phys, 95 (2006) 169–175.
27. N. Obradović, S. Filipović, S. Marković, M. Mitrić, J. Rusmirović, A. Marinković, V. Antić, V. Pavlović, Influence of different pore-forming agents on wollastonite microstructures and adsorption capacities. Ceram Int, 43 (2017) 7461–7468.
28. X. Huang, X. Zhan, C. Wen, F. Xu, L. Luo. Amino-functionalized magnetic bacterial cellulose/activated carbon composite for Pb^{2+} and methyl orange sorption from aqueous solution, J Mater Sci Technol, 34 (2018) 855–863.
29. F. Wei, S. Ma, L. Yang, Y. Feng, J. Z. Wang, A. Hua, X.G. Zhao, D.Y. Geng, Z.D.

Zhang, A new scale for optimized cryogenic magnetocaloric effect in ErAl2@Al2O3 nanocapsules, J Mater Sci Technol, 34 (2018) 848–854.
30. B. Amarababu, V. Pandu Rangadu, Synthesis and Characterization of Mineral Wollastonite Particulate Filled Vinyl-Ester Resin Composites. Int Lett Chem Phys Astron 37 (2013) 91–102.
31. J. D. Rusmirović, N. Obradović, J. Perendija, A. Umićević,A. Kapidžić, B. Vlahović, V. Pavlović, A. D. Marinković, V. B. Pavlović, Controllable synthesis of Fe 3 O 4 - wollastonite adsorbents for efficient heavy metal ions/oxyanions removal. Environ Sci Pollut Res, 26 (2019) 12379–12398.
32. M. I. Khalil, Co-precipitation in aqueous solution synthesis of magnetite nanoparticles using iron(III) salts as precursors. Arab J Chem 8 (2015) 279–284.
33. S. Rajput,, C. U. Pittman,, D. Mohan, J. Colloid Interface Sci., 468 (2016) 334–46.
34. M. A. Ahmed,, S. M. Ali,, S. I. El-Dek,, A. Galal, Mater. Sci. Eng. B Solid-State Mater. Adv. Technol., 178(10) (2013) 744–51.
35. M. Chiban , M. Zerbet, G. Carja and F. Sinan, Application of low-cost adsorbents for arsenic removal: A review, Journal of Environmental Chemistry and Ecotoxicology 4(5) (2012) 91-102.
36. W. H. Höll, Water treatment, Anion Exchangers: Ion Exchange, Encyclopedia of Separation Science (2000) 4477-4484.
37. K. Pantić, Z. J. Bajić, Z. S. Veličković, V. R. Djokić, J. D. Rusmirović, A. D. Marinković, A. Perić-Grujić, Adsorption performances of branched aminated waste polyacrylonitrile fibers: Experimental versus modelling study. Desalin Water Treat, 171 (2019) 223–249.
38. Z. Veličković, G. D. Vuković, A. D. Marinković, M. S. Moldovan, A. A. Perić-Grujić, P. S. Uskoković, M. Dj. Ristić. Adsorption of arsenate on iron(III) oxide coated ethylenediamine functionalized multiwall carbon nanotubes. Chem Eng J, 181-182 (2012) 174–181.
39. E. D. Revellame, D. L. Fortela, W. Sharp, R. Hernandez, M. E. Zappi, Adsorption kinetic modeling using pseudo-first order and pseudo-second order rate laws: A review. Clean Eng Technol 1 (2020) 100032
40. G. Varank, A. Demir, K. Yetilmezsoy, S. Top, E. Sekman, M. S. Bilgili, Removal of 4-nitrophenol from aqueous solution by natural low-cost adsorbents. Indian J Chem Technol, 19 (2012) 7–25.
41. A. Günay, E. Arslankaya, İ. Tosun, Lead removal from aqueous solution by natural and pretreated clinoptilolite: Adsorption equilibrium and kinetics. Journal of Hazardous Materials, 146 (2007) 362-371
42. F. T. Kamga, Modeling adsorption mechanism of paraquat onto Ayous (Triplochiton scleroxylon) wood sawdust, Applied Water Science, 9, (2019) 1.
43. M. E. Mahmoud, M. M. Osman, H. Abdel-Aal, G. M. Nabil, Microwave-assisted adsorption of Cr(VI), Cd(II) and Pb(II) in presence of magnetic graphene oxide-covalently functionalized-tryptophan nanocomposite, J Alloys Compd., 823 (2020) 153855.
44. Y. Wang, G. Morin, G. Ona-Nguema, F. Juillot, G. Calas, G. E. Brown. Distinctive arsenic(V) trapping modes by magnetite nanoparticles induced by different sorption processes, Environ Sci Technol, 45 (2011) 7258–7266.
45. J. Jönsson, D. M. Sherman, Sorption of As(III) and As(V) to siderite, green rust (fougerite) and magnetite: Implications for arsenic release in anoxic groundwaters, Chem Geol 255 (2008) 173–181.
46. J. Perendija, Z. S. Veličković, I. Cvijetić, J. D. Rusmirović, V. Ugrinović, A. D. Marinković, A. Onjia, Batch and column adsorption of cations, oxyanions and dyes on a magnetite modified cellulose-based membrane, Cellulose 27 (2020) 8215–8235.
47. P. R. Grossl, M. Eick, D. L. Sparks, S. Goldberg, C. C. Ainsworth, Kinetic

Evaluation Using a Pressure-Jump Relaxation Technique, Environ Sci Technol, 31 (1997) 321–326.
48. J. S. Markovski, D. D. Marković, V. R. Dokić, M. Mitrić, M. D. Ristić, A. E. Onjia, A. D. Marinković, Arsenate adsorption on waste eggshell modified by goethite, α-MnO_2 and goethite/α-MnO_2, Chem Eng J 237 (2014) 430–442.
49. J. Silva, J. W. V. Mello, M. Gasparon, W. A. P. Abrahão, V. S. T. Ciminelli, T. Jong, The role of Al-Goethites on arsenate mobility, Water Research, 44 (2010) 5684-5692.
50. C-H. Liu, Y-H. Chuang, T-Y Chen, Y. Tian, H. Li, M-K. Wang, W. Zhang, Mechanism of Arsenic Adsorption on Magnetite Nanoparticles from Water: Thermodynamic and Spectroscopic Studies, Environ Sci Technol, 49 (2015) 7726–7734.
51. Y. Ge, X. Cui, C. Liao, Z. Li, Facile fabrication of green geopolymer/alginate hybrid spheres for efficient removal of Cu(II) in water: Batch and column studies, Chem Eng J, 311 (2017) 126–134.
52. M. Karanac, M. Đolić, Z. Veličković, A. Kapidžić, V. Ivanovski, M. Mitrić, A. Marinković, Efficient multistep arsenate removal onto magnetite modified fly ash, J Environ Manage, 224 (2018) 263–276.
53. V. Nikolić, N. Tomić, M. Bugarčić, M. Sokić, A. Marinković, Z. Veličković, Ž. Kamberović, Amino-modified hollow alumina spheres: effective adsorbent for Cd^{2+}, Pb^{2+}, As(V), and diclofenac removal, Environ Sci Pollut Res 2021.
54. K. Taleb, J. Markovski, Z. Veličković, J. Rusmirović, Milica Rančić, V. Pavlović, A. Marinković, Arsenic removal by magnetite-loaded amino modified nano/microcellulose adsorbents: Effect of functionalization and media size, Arabian Jouranl Of Chemisrty, 12 (2019) 4675-4693.
55. M. Usman, I. Katsoyiannis, M. Mitrakas, A. Zouboulis, M. Ernst, Performance evaluation of small sized powdered ferric hydroxide as arsenic adsorbent, Water (Switzerland) 10 (2018) 1–15.
56. P. R. Sharma, S. K. Sharma, R. Antoine, B. S. Hsiao, Efficient Removal of Arsenic Using Zinc Oxide Nanocrystal-Decorated Regenerated Microfibrillated Cellulose Scaffolds, ACS Sustain Chem Eng, 7 (2019) 6140–6151.
57. An, B., Liang, Q., Zhao, D., 2011. Removal of arsenic(V) from spent ion exchange brine using a new class of starch-bridged magnetite nanoparticles, Water Res., 45 (2011), 1961–1972.
58. L. Du, P. Gao, Y. Meng, Y. Liu, S. Le, C. Yu, Highly Efficient Removal of Cr(VI) from Aqueous Solutions by Polypyrrole/Monodisperse Latex Spheres, ACS Omega 5 (2020) 6651–6660.
59. M. Bhaumik, S.Agarwal, V. K. Gupta, A. Maity, Enhanced removal of Cr(VI) from aqueous solutions using polypyrrole wrapped oxidized MWCNTs nanocomposites adsorbent, Journal of Colloid and Interface Science, 470 (2016) 257-267.

Сажетак: *У овом раду је окарактерисана структура, морфологија и састав синтетизованог композита магнетит/3D штампан воластонит (3D_W) и проучаване су његове адсорпционе перформансе у односу на As(V) и Cr(VI). Магнетитом (МГ) модификовани 3D штампани воластонит је добијен поступком у два корака: модификацијом 3D_W са 3-аминопроилсиланом (АПТЕС) праћеном контролисаним таложењем магнетита (МГ) да би се добио 3Д_В/М адсорбент. Структура/особине 3D_W/M су потврђене применом ФТИР, КСРД, ТГД/ДТА и СЕМ анализе. Адсорпциона својства хибридних адсорбената су спроведена за уклањање As(V) и Cr(VI) – једно у односу на почетну pH вредност, масу адсорбента, температуру и време адсорпције. Студија адсорпције зависне од времена најбоље је описана једначином псеудо-другог реда, док је Вебер Морисова анализа показала да дифузија унутар честица*

контролише дифузиони транспорт. Слична енергија активације, 17,44 и 14,49 kJ•mol^{-1} *за адсорпцију As(V) и Cr(VI) на 3D_W/M, респективно, указује на главни допринос физичке адсорпције. Одређивање параметара адсорпције извршено је применом различитих модела изотерме адсорпције, а најбоље уклапање добијено је коришћењем Фројндлиховог модела. Добијени су адсорпциони капацитети од 24,16 и 29,6 mg g^{-1} за As(V) и Cr(VI) на 2^{o}C, Co = 5,5 и 5,3 mg L^{-1}. Термодинамичка студија је показала повољан процес на вишој температури. Прелиминарна студија са фиксном колоном и резултати који су усклађени са Бохарт-Адамсом, Јон-Нелсоном, Тхомасом и модификованим моделом доза-одговор показали су добро слагање са резултатима серије серије.*

***Кључне речи**: арсен, хром, адсорпција, магнетит, 3 D штампа воластонит.*